Rev. Adv. Mater. Sci. 35 (2013) 96-103

FORMATION OF NANOSCOPIC GRAINS DUE TO DISLOCATION PILE-UP TRANSFORMATIONS IN DEFORMED ULTRAFINE-GRAINED MATERIALS

I.A. Ovid'ko[1,2,3] and N.V. Skiba[1,2]

[1]Department of Mathematics and Mechanics, St. Petersburg State University, Universitetskii pr. 28, Staryi Peterhof, St. Petersburg 198504, Russia
[2]Institute of Problems of Mechanical Engineering, Russian Academy of Sciences, Bolshoj 61, Vasil. Ostrov, St. Petersburg 199178, Russia
[3] St. Petersburg State Polytechnical University, St. Petersburg 195251, Russia

Received: September 31, 2013

Abstract. A new mechanism/mode of plastic deformation in ultrafine- and coarse-grained polycrystalline materials is theoretically described which occurs through nanograin formation induced by stress fields and transformations of dislocation pile-ups. It is demonstrated that lattice dislocations of a pile-up stopped at a grain boundary (GB) are trapped at the GB and transform into GB dislocations. The GB dislocations climb, and this leads to formation of a locally non-equilibrium GB fragment with tilt misorientation different from that of its neighboring (equilibrium) grain boundary fragments. The locally non-equilibrium GB fragment under shear stress splits into an immobile GB segment and mobile GB segment that moves within an adjacent ultrafine grain, in which case a new nanoscopic grain within the ultrafine grain is formed. Our theory is consistent with the corresponding experimental data reported in the literature.

1. INTRODUCTION

Ultrafine-grained (UFG) and nanocrystalline materials characterized by superior strength represent the subject of rapidly growing research efforts motivated by a wide range of their current and potential applications; see, e.g., [1-24]. The UFG structure in bulk metallic materials is typically formed due to severe plastic deformation that causes grain refinement in initially coarse-grained structures. In order to control the final UFG structure in severely deformed materials, it is highly interesting to understand and describe both the nature and micromechanisms for deformation-induced grain refinement. Despite of the progress in this area [25,26], micromechanisms for deformation-induced grain refinement are still the subject of intense debates. Formation of the UFG structure during plastic deformation is conventionally treated to occur through continuous evolution of lattice dislocation ensembles; see, e.g., reviews [25,26]. This evolution involves generation of dislocation walls, dislocation cell subboundaries and their further continuous transformation into high-angle GBs under mechanical load. The discussed representations on grain refinement through continuous evolution of dislocation ensembles are well consistent with numerous experimental data; see reviews [25,26] and references therein.

At the same time, there are experimental data and computer simulation results that can not be explained within the approach operating with continuous evolution of dislocation ensembles. For instance, in the experiment by Wu with coworkers [27], nanograin nucleation was observed at GBs and their triple junctions in comparatively large grains of cobalt under surface mechanical treatment. In order to explain this phenomenon, it is reasonable to ex-

Corresponding author: I.A. Ovid'ko, e-mail: ovidko@nano.ipme.ru

ploit ideas on generation of nanograins through splitting and migration of GBs; see computer simulations [28] and theoretical models [29-31]. In doing so, computer simulations [28] have shown nanograin nucleation at triple junctions of GBs, and theoretical models [29-31] have also described nanograin nucleation in vicinities of triple junctions where high local stresses and special defects – GB disclinations creating such stresses - are often generated during intergranular plastic deformation. However, in addition to nanograin formation at triple junctions, the same formation process was experimentally observed at straight GB fragments distant enough from triple junctions [27]. The main aim of this paper is to suggest a theoretical model describing the experimentally observed [27] nanograin nucleation at straight GB fragments in UFG materials. Within the suggested approach, a new nanograin is generated due to transformations of dislocation pile-ups stopped by GBs.

2. STRESS-DRIVEN NUCLEATION OF NANOGRAINS DUE TO TRANSFORMATIONS OF DISLOCATION PILE-UPS: GENERAL ASPECTS AND GEOMETRY

Let us consider geometric features of plastic deformation mode occurring through stress-driven nucleation of nanograins due to transformations of dislocation pile-ups in ultrafine-grained (UFG) materials. Fig. 1a schematically shows a two-dimensional section of an UFG solid consisting of ultrafine grains divided by GBs. The solid is under mechanical load and contains a pileup of lattice edge dislocations stopped by GB $A'B'$ (Figs. 1a and 1b). The dislocations are characterized by the Burgers vector magnitude b and hereinafter called b-dislocations. The head dislocation of the pile-up in its initial state under consideration is trapped by the GB $A'B'$ (Fig. 1b). Within our model, the head dislocation splits into several GB dislocations (Fig. 1 c). This splitting process is rather typical in various materials (see, e.g., [32,33] and references therein), because it reduces the elastic energy of the dislocation. The splitting of the GB dislocation into several GB dislocations involves, in particular, their diffusion-controlled climb along the GB $A'B'$ (Fig. 1c).

After the splitting of the head dislocation, the second dislocation of the pile-up moves towards the GB layer $A'B'$ where it is trapped (Fig. 1d) and then splits into several GB dislocations (Fig. 1e). The process in question repeatedly occurs and leads to formation of a GB dislocation wall AB of finite extent at the GB $A'B'$ (Fig. 1f). That is, as a result of the consequent splitting processes of dislocations belonging to the pile-up, a locally non-equilibrium GB is formed which has a local segment AB specified by a high density of extra GB dislocations (Fig. 1f). In a first approximation, we assume that the density of the extra GB dislocations is constant at the GB fragment AB of length L (Fig. 1f). In the circumstances discussed, for the aims of our further analysis focused on strain energy characteristics of the extra GB dislocations, the GB dislocation wall AB is effectively represented as a dipole of wedge disclinations located at points A and B and specified by disclination strengths $\pm\Omega$ unambiguously defined by parameters (Burgers vector and period) of the wall of the extra GB dislocations (Fig. 1g). Hereinafter, such disclinations will be called $\pm\Omega$ -disclinations. This representation based on the theory of disclinations in solids [34] simplifies our analysis and, at the same time, catches all the essential aspects of the problem under examination.

In the framework of the suggested model, following the approach [29-31], formation of a new nanograin at the GB $A'B'$ occurs through stress-driven splitting of the GB fragment AB into an immobile fragment AB and a mobile GB fragment CD that migrates within the adjacent grain (Fig. 1h). In terms of disclinations, this process is described as stress-driven splitting of the dipole AB of $\pm\Omega$ - disclinations into an immobile dipole AB of $\pm(\Omega - \omega + \Delta)$ - disclinations (wedge disclinations specified by strengths $\pm(\Omega - \omega + \Delta)$ and a mobile dipole CD of $\pm(\omega - \Delta)$-disclinations (wedge disclinations specified by strengths $\pm(\omega - \Delta)$) that move within the adjacent grain (Fig. 1h). Here Δ is the tilt misorientation of GB segments AC and BD that are formed due to shear coupled to stress-driven migration of GB CD.

More precisely, in spirit of the approach [35-40], when the GB CD migrates under the shear stress action, plastic shear coupled to the migration can occur in direction parallel with the GB CD (Fig. 1h). The coupled shear is localized within the region $ABCD$ swept by the migrating GB CD, in which case the shear is unfinished at the segments AC and BD. As a corollary, in the general situation, the segments AC and BD can be viewed as finite walls of noncrystallographic dislocations whose Burgers vectors are associated with the unfinished shear (Fig. 1h). The finite walls of noncrystallographic dislocations AC and BD in their turn are logically treated as GB dislocation segments specified by

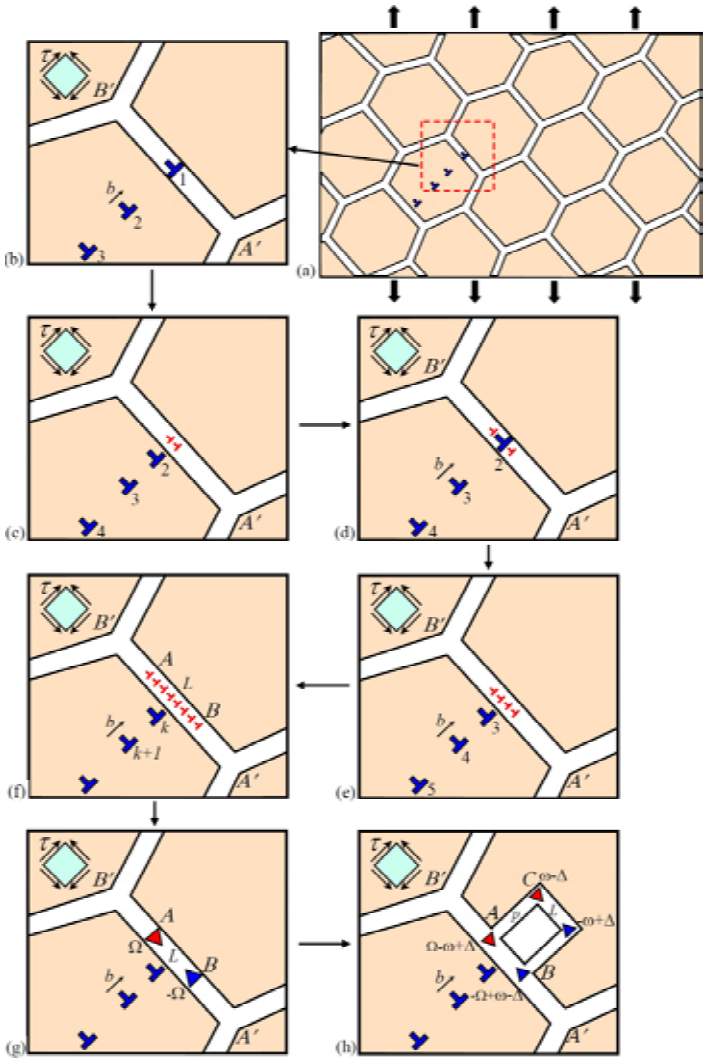

Fig. 1. Formation of both locally non-equilibrium grain boundary and new nanograin at this boundary due to transformations of dislocation pile-up in ultrafine-grained solid (schematically). (a) A two-dimensional section of an ultrafine-grained specimen consisting of ultrafine grains divided by grain boundaries. The specimen is under tensile load and contains a pileup of lattice edge dislocations stopped by grain boundary $A'B'$. Figures (b-e) highlight both evolution of the pile-up of lattice dislocations through their transformations to grain boundary dislocations and formation of new nanograin. (b) The head dislocation (1) of the pile-up in its initial state is trapped by the grain boundary $A'B'$. (c). The head dislocation splits into several grain boundary dislocations The splitting process involves, in particular, diffusion-controlled climb of grain boundary dislocations along the grain boundary $A'B'$. (d) After the splitting of the head dislocation, the second dislocation (2) of the pile-up moves towards the grain boundary layer $A'B'$ where it is trapped. (e) Then the second dislocation splits into several grain boundary dislocations. (f) The splitting processes repeatedly occur and lead to formation of a grain boundary dislocation wall AB of finite extent at the grain boundary $A'B'$. That is, as a result of the consequent splitting processes of dislocations belonging to the pile-up, a locally non-equilibrium grain boundary is formed which has a local segment AB specified by a high density of extra grain boundary dislocations. (g) The finite wall of extra grain boundary dislocations is modeled as a dipole of wedge $\pm\Omega$-disclinations (triangles) A and B. (h) The dipole of $\pm\Omega$-disclinations splits into immobile dipole of $\pm(\Omega - \omega + \Delta)$-disclinations ($A$ and B) and mobile dipole of $\pm(\omega - \Delta)$-disclinations (C and D) that move in adjacent grain interior over the distance p. As a result, new nanograin $ABCD$ is formed; for details, see text.

the tilt misorientation Δ which, in the context discussed, characterizes the shear coupled to stress-driven migration of GB CD.

(Note that, in general, both the situations with $\Omega + \Delta > \omega$ and $\Omega + \Delta < \omega$ can come into play during the nanograin formation process. In our further

calculations, both these situations are automatically taken into account. At the same time, for definiteness, Fig. 1h illustrates the only former situation where the nanograin formation process produces immobile disclinations specified by the strengths $\Omega - \omega + \Delta$ and $-(\Omega - \omega + \Delta)$ (Fig. 1h) having the same sign as the strengths Ω and $-\Omega$ of the initial disclinations located at *A* and *B*, respectively (Fig. 1g).)

Thus, according to our model, formation of a new nanograin at the GB *A′B′* occurs through stress-driven splitting of the GB fragment *AB* into an immobile fragment *AB* and a mobile GB fragment *CD* that migrates within the adjacent grain and produces GB segments *AC* and *BD* due to the unfinished plastic shear coupled to the migration process (Fig. 1h). As a result, the new nanograin *ABCD* is formed (Fig. 1h). Also, the migration of the GB segment *CD* with wedge disclinations (specified by strengths $\pm(\omega - \Delta)$ at its vortices, *C* and *D*, over the distance *p* carries plastic flow characterized by both *p* and the disclination strengths $\pm(\omega - \Delta)$. The plastic deformation work under the shear stress serves as the key driving force for the new nanograin formation. The generation of the new disclinations at vortices *A*, *B*, *C,* and *D* contributes to the hampering force for the new nanograin formation. So does the formation of the new GB segment *AC* and *BD* whose energies should be taken into account in the hampering force.

The nanograin *ABCD* formation (Figs. 1g and 1h) is characterized by the energy change $\Delta W = W_2 - W_1$ of the defect configuration. Here W_1 and W_2 are the energies of the defect configuration in its initial and final states, respectively (see Figs. 1g and 1h, respectively). The nanograin formation is energetically favorable, if $\Delta W < 0$. Let us calculate the energy change ΔW which has the nine basic terms:

$$\Delta W = E_2^{\omega} + E_2^{\Omega} - E_1^{\Omega} + E_2^{\omega-\Omega} + E_2^{\omega-c} + E_2^{\Omega-c} - E_1^{\Omega-c} + E_{\Sigma}^{\gamma} + E^{\tau}, \quad (1)$$

where E_1^{Ω}, E_2^{ω}, and E_2^{Ω} are the proper energies of the dipoles of $\pm\Omega$-disclinations, $\pm(\omega - \Delta)$-disclinations and $\pm(\Omega - \omega + \Delta)$-disclinations, respectively; $E_2^{\omega-\Omega}$ is the energy of the elastic interaction between the dipole of $\pm(\omega - \Delta)$-disclinations and the dipole of $\pm(\Omega - \omega + \Delta)$-disclinations; $E_1^{\Omega-c}$, $E_2^{\omega-c}$, and $E_2^{\Omega-c}$ are the energies that specify the elastic interaction between the pile-up of lattice *b*- dislocations and the dipoles of $\pm\Omega$-disclinations, $\pm(\omega - \Delta)$-disclinations and $\pm(\Omega - \omega + \Delta)$-disclinations, respectively; E_{Σ}^{γ} is the sum specific energy of the GBs *BC*, *AD* and *CD*; and E^{τ} is the work spent by the external shear stress τ on movement of the dipole of $\pm(\omega - \Delta)$-disclinations over the distance *p*.

Following [41], the proper energies, E_1^{Ω}, E_2^{ω}, and E_2^{Ω}, of the disclination dipoles are given as follows:

$$E_1^{\Omega} = \frac{D\Omega^2 L^2}{2}\left(\ln\frac{R}{L} + \frac{1}{2}\right), \quad (2)$$

$$E_2^{\omega} = \frac{D(\omega - \Delta)^2 L^2}{2}\left(\ln\frac{R}{L} + \frac{1}{2}\right), \quad (3)$$

$$E_2^{\omega} = \frac{D(\Omega - \omega + \Delta)^2 L^2}{2}\left(\ln\frac{R}{L} + \frac{1}{2}\right), \quad (4)$$

where $D = G[2\pi(1 - \nu)]$ (with *G* being the shear modulus and ν being the Poisson ratio), and *R* is the screening radius for stress fields created by the disclination dipoles.

The energy $E_2^{\omega-\Omega}$ of the elastic interaction between the dipole of $\pm(\omega - \Delta)$-disclinations and the dipole of $\pm(\Omega - \omega + \Delta)$-disclinations can be written by the following formula obtained from expressions presented in Refs. [29,42]:

$$E_2^{\omega-\Omega} = \frac{D(\omega - \Delta)(\Omega - \omega + \Delta)}{2} \times \left(L^2 + L^2 \ln\frac{R^2}{L^2 + p^2} - p^2 \ln\frac{L^2 + p^2}{p^2}\right). \quad (5)$$

The interaction energies $E_1^{\Omega-c}$, $E_2^{\omega-c}$, and $E_2^{\Omega-c}$ are calculated as the works spent to generation of the pile-up of lattice *b*- dislocations in the stress fields created by the dipoles of $\pm\Omega$-disclinations, $\pm(\omega - \Delta)$-disclinations, and $\pm(\Omega - \omega + \Delta)$-disclinations, respectively; see, e.g., [43]. In doing so, we find:

$$E_1^{\Omega-c} = \frac{Db\Omega L}{2}\sum_{i=1}^{n_c}\ln\frac{L^2 + 4(R + x_i)^2}{L^2 + 4x_i^2}, \quad (6)$$

$$E_1^{\omega-c} = \frac{Db(\omega - \Delta)L}{2}\sum_{i=1}^{n_c}\ln\frac{L^2 + 4(R + x_i)^2}{L^2 + 4x_i^2}, \quad (7)$$

$$E_1^{\omega-c} = \frac{Db(\Omega - \omega + \Delta)L}{2} \times \sum_{i=1}^{n_c}\ln\frac{L^2 + 4(R + x_i + p)^2}{L^2 + 4(x_i + p)^2}, \quad (8)$$

where n_c is the number of *b*-dislocations in the pile-up, $x_i = lag_i/\tau$ are the coordinates of equilibrium po-

sitions of the *b*-dislocations composing the pile-up, and lag_j are the Laguerre coefficients [44].

We assume that the GBs *BC*, *AD,* and *CD* are characterized by the same specific (per unit area) energy γ_{gb} whose value is typical for high-angle GBs. With this assumption, the sum specific energy of the GBs *BC*, *AD,* and *CD* is as follows:

$$E_{\Sigma}^{\gamma} = (2p + L)\gamma_{gb}. \quad (9)$$

The energy E^{τ} is calculated as the following work spent by the external shear stress τ on movement of the dipole of $\pm(\omega - \Delta)$-disclinations over the distance *p*:

$$E^{\tau} = -\tau(\omega - \Delta)pL. \quad (10)$$

With formulas (1)-(10), the total energy change ΔW is written as:

$$\Delta W = \frac{D(\omega - \Delta)(\Omega - \omega + \Delta)}{2} \times \left(L^2 \ln\frac{L^2 + p^2}{L^2} + p^2 \ln\frac{L^2 + p^2}{p^2} \right) - \frac{Db(\omega - \Delta)L}{2} \sum_{i=1}^{n_c} \ln\left[1 + \frac{p^2 + 2px_i}{(L/2)^2 + x_i^2} \right] - \tau(\omega - \Delta)pL + (2p + L)\gamma_{gb}. \quad (11)$$

Let us analyze the energy change ΔW (given by formula (11)) as a function of parameters characterizing the system under consideration. To do so, in the exemplary cases of ultrafine-grained Co (cobalt), Al (aluminum), and α-Al_2O_3 (saphire), we calculate the energy change ΔW as a function of both the disclination strength ω of the mobile dipole *CD* of $\pm(\omega - \Delta)$-disclinations and the distance *p* moved by the migrating GB *CD*, for various values of the misorientation parameter Δ. In our calculations, we exploit the following characteristics of materials under examination: G = 75 GPa, ν = 0.31, b_{Co} = 0.204 nm [45], and γ_{gb}^{Co} = 0.7 J/m^2 [45], in the case of Co; G = 26.5 GPa, ν = 0.34, b_{Al} = 0.286 nm [46], and γ_{gb}^{Al} = 0.4J/m^2 [47], in the case of Al; and G = 169 GPa, ν = 0.23 [48], b_{Al2O3}= 0.475 nm [49], and $\gamma_{gb}^{Al_2O_3}$ = 0.5 J/m^2 [50], in the case of α-Al_2O_3. Values of other parameters characterizing the system are taken as: Ω = 5°, τ = 0.7 GPa, for Co; τ = 0.5 GPa, for Al; and τ = 1.0 GPa, for α-Al_2O_3.

We calculated the dependences $\Delta W(\omega,p)$ and presented them as maps in Fig. 2, for n_c = 5 and L = 5 nm, and Fig. 3, for n_c = 20 and L = 20 nm a. As it follows from the maps (Figs. 2 and 3), the nanograin formation associated with the splitting of disclinations (Fig. 2 and Fig. 3) is energetically favorable, if the disclination strength w is in the range of $\omega_{C1} < \omega < \omega_{C2}$, where ω_{C1} and ω_{C2} are some critical values. Also, when D grows, the interval of "favorable" values of ω (values at which thew nangrain formation is energetically favorable) shifts towards large values of ω. For instance, for Δ = 0.3, one has 22°< ω <56° in the case of Co (Fig. 2a), 22°< ω <55° in the case of Al (Fig. 2b), and 21°< ω <60° in the case of α-Al_2O_3 (Fig. 2c). At the same time, for Δ = 0.5, we have 34°< ω <67° in the case of Co (Fig. 2d), 36°< ω <66° in the case of Al (Fig. 2e) and 32°< ω <71° in the case of α-Al_2O_3 (Fig. 2f). Note that the discussed intervals for ultrafine-grained ceramic α-Al_2O_3 (21°< ω <60° and 32°< ω <71°; see Figs. 2c and 2f, respectively) are wider than those (22°< ω <56° and 26°< ω <55°, and 34°< ω <67° and 36°< ω <66°; see Figs. 2a and 2b, and Figs. 2d and 2e, respectively) for ultrafine-grained metals, Co and Al.

Also, the maps presented in Fig. 2 and Fig. 3 are indicative of the fact that the migration of the GB *CD* is energetically favorable until the distance *p* moved by this GB reaches some equilibrium value of p_{eq}, corresponding to a local minimum of the function $\Delta W(p)$. For instance, in the case of ultrafine-grained Co, the equilibrium distance p_{eq} = 16 nm, for ω = 23°, n_c = 5, and L = 5 (Fig. 2a), and p_{eq} = 16 nm, for ω = 36°, n_c = 20, and L = 20 (Fig. 3a). Thus, with these values, the new nanograin *ABCD*, in the former case (Fig. 2a), represents an elongated rectangular grain with linear sizes 5 nm and 16nm (Fig. 2a) and, in the second case (Fig. 3a), is approximately equiaxial rectangular grain having sizes 20 nm and 16 nm. The latter case predicted in our theoretical work is well consistent with the experimental observation [27] of nanograins nucleated at GBs in Co and specified by approximately equiaxial shape with linear sizes being around 20 nm.

Let us calculate dependences of the energy change ΔW on the nanograin width L at the same values of parameters characterizing the system, as with the previous situation, and for ω = 30°, Δ = 0.3, and p = 2 nm. These dependences are presented in Fig. 4 for n_c = 5 (Fig. 4a) and n_c = 20 (Fig. 4b) in the cases of ultrafine-grained Al (curve 1), Co (curve 2) and α-Al_2O_3 (curve 3). As it follows from Fig. 4, when the nanograin width L (or, in other terms, the size of a local non-equilibrium GB fragment generated due to transformations of a dislocation pile-up; see Fig. 1 a-e) increases, the nanograin formation is hampered. At some critical value of $L = L_c$, the

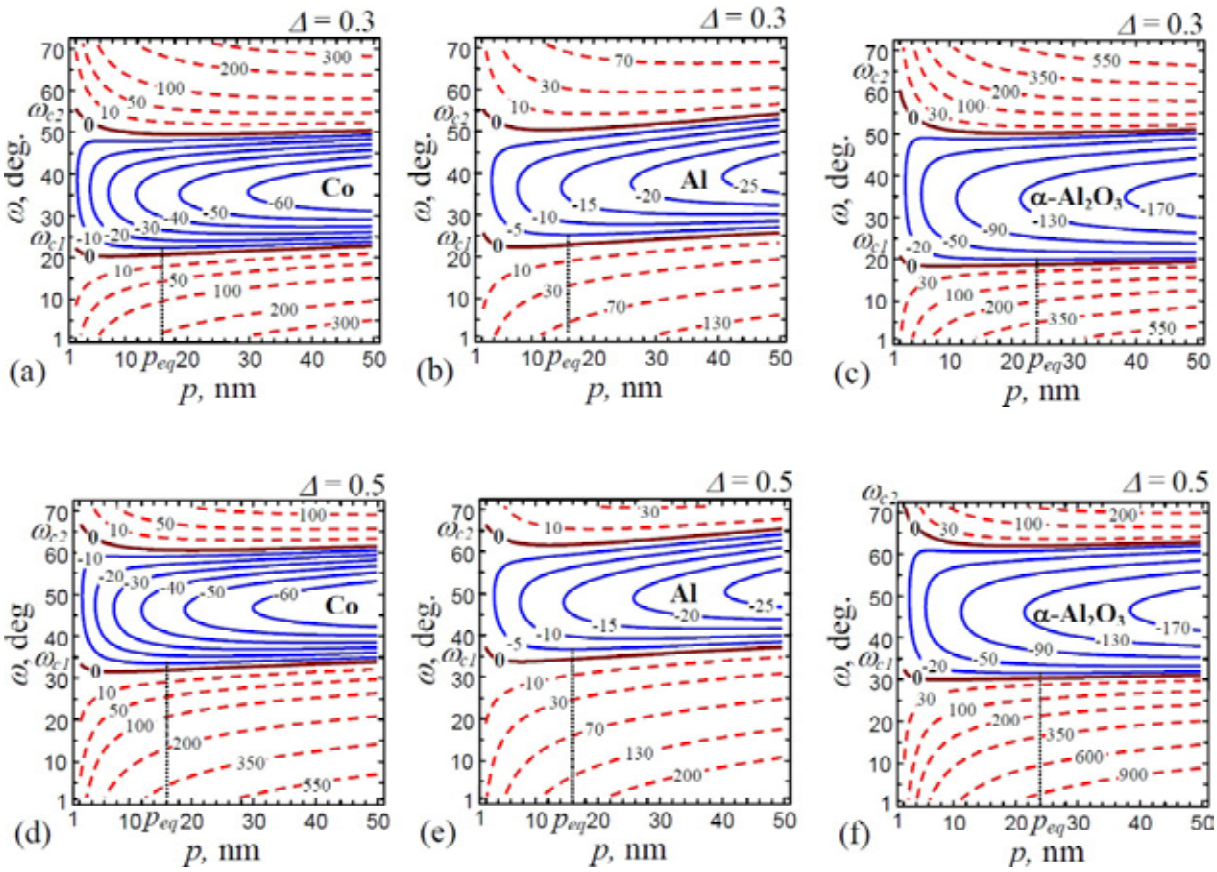

Fig. 2. Dependences (maps) of the energy change ΔW on both the disclination strength ω of mobile dipole of $\pm(\omega - \Delta)$-disclinations and the distance p moved by this dipole, for various values of the misorientation parameter Δ and n_c = 5 nm, L = 5 nm in the cases of Co (a, d), Al (b, e), and α-Al_2O_3 (c, f).

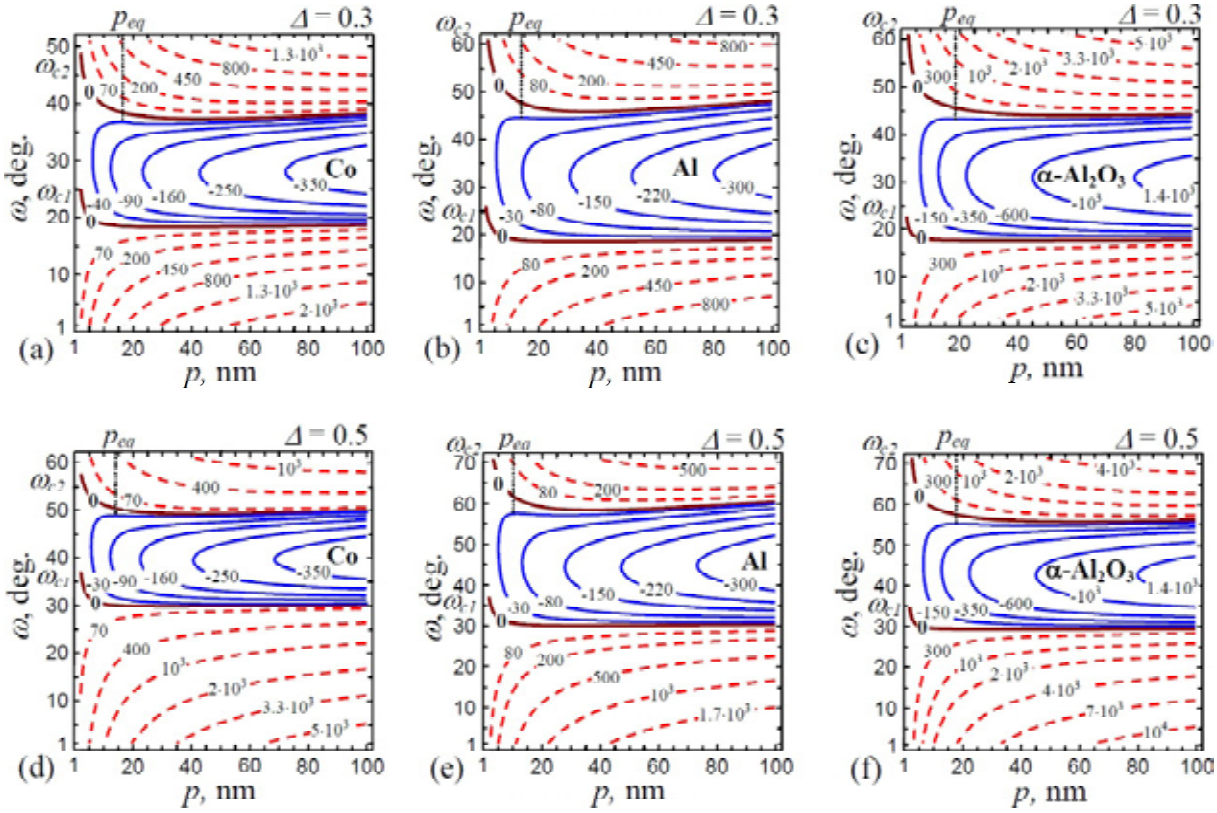

Fig. 3. Dependences (maps) of the energy change ΔW on both the disclination strength ω of mobile dipole of $\pm(\omega - \Delta)$-disclinations and the distance p moved by this dipole, for various values of the misorientation parameter Δ and n_c = 20 nm, L = 20 nm in the cases of Co (a, d), Al (b, e) and α-Al_2O_3 (c, f).

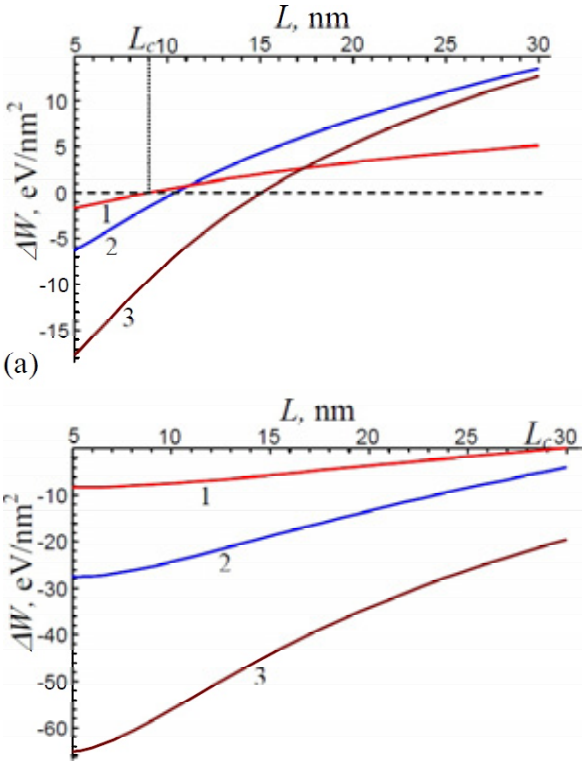

Fig. 4. (Color online) Dependences of energy change ΔW on nanograin width L in the cases of nanocrystalline Al (curve 1), Co (curve 2) and α-Al_2O_3 (curve 3).

nanograin formation becomes energetically unfavorable.

3. CONCLUDING REMARKS

Thus, the nanograin nucleation through splitting of dislination dipoles generated at locally non-equilibrium GBs (Fig. 1) is energetically favorable in wide ranges of parameters of deformed ultrafine-grained materials. Within our model, locally non-equilibrium GBs are effectively generated during stoppage of pile-ups of lattice dislocations by GBs where these dislocations split into climbing GB dislocations (Figs. 1a-1e). Besides, splitting of dislination dipoles generated at locally non-equilibrium GBs (Figs. 1h and 1g) is effectively enhanced by the stress field created by the dislocation pile-up stopped by the GB. That is, the dislocation pile-up plays a double role: it creates locally non-equilibrium GB structure and generates stresses that drive the nanograin nucleation at the locally non-equilibrium GB. In doing so, lattice dislocations of the pile-up effectively initiate plastic flow through stress-driven migration of GBs and thus transform lattice slip to plastic deformation on the nanograin level, that is, plastic deformation carried by newly nucleated grain. The suggested theoretical representations on plastic flow occurring through nucleation of nanograins at GBs in ultrafine-grained materials are well consistent with both the experimental observation [27] of nanograins nucleated at GBs in cobalt.

ACKNOWLEDGEMENTS

IAO and NVS were supported by the Ministry of Education and Science of the Russian Federation (Grant 14.B25.31.0017) and St. Petersburg State University research grant 6.37.671.2013. Also, NVS was supported by the Russian Foundation of Basic Research (grant 12-02-31642-mol-a).

REFERENCES

[1] A.K. Mukherjee // *Mater. Sci. Eng.* A **322** (2002) 1.
[2] R.Z. Valiev // *Nature Mater.* **3** (2004) 511.
[3] S.V. Bobylev, M.Yu. Gutkin and I.A. Ovid'ko // *Phys. Rev. B* **73** (2006) 064102.
[4] M.Yu. Gutkin and I.A. Ovid'ko // *Appl. Phys. Lett.* **88** (2006) 211901.
[5] M. Dao, L. Lu, R.J. Asaro, J.T.M. De Hosson and E. Ma // *Acta Mater.* **55** (2007) 4041.
[6] A. Mukhopadhyay and B. Basu // *Int. Mater. Rev.* **52** (2007) 257.
[7] M. Kawasaki and T.G. Langdon // *J. Mater. Sci.* **42** (2007) 1782.
[8] C.C. Koch, I.A. Ovid'ko, S. Seal and S. Veprek, *Structural Nanocrystalline Materials: Fundamentals and Applications* (Cambridge, Cambridge University Press, 2007).
[9] E.C. Aifantis // *Mater. Sci. Eng.* A **503** (2009) 190.
[10] C.S. Pande and K.P. Cooper // *Progr. Mater. Sci.* **54** (2009) 689.
[11] R.Z. Valiev, M.Yu. Murashkin, A. Kilmametov, B. Straumal, N.Q. Shinh and T.G. Langdon // *J. Mater. Sci.* **45** (2010) 4718.
[12] R.Z. Valiev and T.G. Langdon // *Adv. Eng. Mater.* **12** (2010) 677.
[13] H.A. Padilla II and B.L. Boyce // *Exp. Mechanics* **50** (2010) 5.
[14] I.A. Ovid'ko // *Mater. Phys. Mech.* **12** (2011) 76.
[15] I.A. Ovid'ko and A.G. Sheinerman // *Rev. Adv. Mater. Sci.* **29** (2011) 105.
[16] I.A. Ovid'ko and A.G. Sheinerman // *Rev. Adv. Mater. Sci.* **27** (2011) 189.
[17] I.A. Ovid'ko, A.G. Sheinerman and E.C. Aifantis // *Mater. Phys. Mech.* **12** (2011) 1.

[18] F. Cleri // *Int. J. Plasticity* **37** (2012) 31.
[19] O. Sitdikov, S. Krymskiy, M. Markushev, E. Avtokratova and T. Sakai // *Rev. Adv. Mater. Sci*. **31** (2012) 62.
[20] N.F. Morozov, I.A. Ovid'ko, A.G. Sheinerman and N.V. Skiba // *Rev. Adv. Mater. Sci.* **32** (2012) 75.
[21] I.A. Ovid'ko and T.G. Langdon // *Rev. Adv. Mater. Sci*. **30** (2012) 103.
[22] I.A. Ovid'ko and A.G. Sheinerman // *Rev. Adv. Mater. Sci*. **32** (2012) 61.
[23] I.A. Ovid'ko and N.V. Skiba // *Scr. Mater*. **67** (2012) 13.
[24] R.Z. Valiev, I. Sabirov, A.P. Zhilyaev and T.G. Langdon // *JOM*. **64** (2012) 1134.
[25] Y. Estrin and A. Vinogradov // *Acta Mater*. **61** (2013) 782.
[26] T. Sakai, A. Belyakov, R. Kaibyshev, H. Miura and J.J. Jonas // *Prog. Mater. Sci*. **60** (2014) 130.
[27] X. Wu, N. Tao, Y. Hong, G. Liu, B. Xu, J. Lu and K. Lu // *Acta Mater*. **53** (2005) 681.
[28] V. Yamakov, D. Wolf, S.R. Phillpot and H. Gleiter // *Acta Mater*. **50** (2002) 5005.
[29] S.V. Bobylev and I.A. Ovid'ko // *Appl. Phys. Lett*. **92** (2008) 081914;
[30] I.A. Ovid'ko, N.V. Skiba, and A.K. Mukherjee // *Scr. Mater*. **62** (2010) 387.
[31] S.V. Bobylev, N.F. Morozov and I.A. Ovid'ko // *Phys. Rev. B* **84** (2011) 094103
[32] P.H. Pumphrey and H. Gleiter // *J. Microscopy* **103** (1974) 349.
[33] A.A. Nazarov // *Interface Sci.* **8** (2000) 71.
[34] A.E. Romanov and A.L. Kolesnikova // *Prog. Mater. Sci*. **54** (2009) 740.
[35] J.W. Cahn and J.E. Taylor // *Acta Mater*. **52** (2004) 4887.
[36] J.W. Cahn, Y. Mishin and A. Suzuki // *Acta Mater*. **54** (2006) 4953.
[37] J.W. Cahn, Y. Mishin and A. Suzuki // *Philos. Mag*. **86** (2006) 3965.
[38] F. Sansoz and V. Dupont // *Appl. Phys. Lett.* **89** (2006) 111901.
[39] J. Schafer and K. Albe // *Acta Mater*. **60** (2012) 6076.
[40] J.J. Li and A.K. Soh // *Appl. Phys. Lett*. **101** (2012) 241915.
[41] A.E. Romanov and V.I. Vladimirov, In: *Dislocations in Solids*, edited by F.R.N. Nabarro (North Holland, Amsterdam, 1992) p. 191.
[42] N.F. Morozov, I.A. Ovid'ko and N.V. Skiba // *Rev. Adv. Mater. Sci.* **29** (2011) 180.
[43] M.Yu. Gutkin, I.A. Ovid'ko and N.V. Skiba // Acta Mater. **51** (2003) 4059.
[44] J.D. Eshelby, F.C. Frank, F.R.N. Nabarro // *Phil. Mag*. **42** (1951) 351.
[45] M.S. Wu, A.A. Nazarov and K. Zhou // *Phil. Mag*. **84** (2004) 785.
[46] J.P. Hirth and J. Lothe, *Theory of dislocations* (Wiley, New York, 1982).
[47] G.C. Hasson and C. Goux // *Scripta Metall.* **5** (1971) 889.
[48] C.J. Smithells and E.A. Brands, *Metals reference book* (Butter-worths, London, 1976).
[49] H. Heuer, K.P.D. Lagerloft and J. Castaing // *Phil. Mag. A* **78** (1998) 747.
[50] T. Watanabe, H. Yoshida, T. Saito, T. Yamamoto, Y. Ikuhara and T. Sakuma // *Mater. Sci. Forum* **304-306** (1999) 601.